Nanopolaritonics with a continuum of molecules: Simulations of molecular-induced selectivity in plasmonics transport through a continuous Y-shape

Daniel Neuhauser
Department of Chemistry and Biochemistry, UCLA, 607 Charles E. Young Avenue, Los Angeles, California 90095-1569, USA

(Received 16 September 2011; accepted 2 November 2011; published online 29 November 2011)

Using the recent NF (near-field) formulation for electrodynamics on the nanoscale, we simulate transport in a Y-shape gold nanostructure in the presence of 2-level molecules. NF is shown to be easily integrated with the Liouville equation, producing a simple and efficient nanopolaritons (plasmons-excitons) solver, with a large time step. Two cases are considered: coating of the gold structure with molecular layers thinner than the structure, and filling space with aligned molecules. In both cases significant effects on the radiation transport are obtained even for low molecular densities. At low densities the effects are primarily an overall reduction of the plasmonics peak, but at higher densities there is a significant selectivity control by the molecules. A redshift is predicted, especially for the space-filling case. The combined nanopolariton shows qualitative hybridization, and the spectral peaks separate with increasing coupling, i.e., with increasing molecular densities. The results open the way to "control of light by light," i.e., controlling plasmonic light transport by inducing a change in the direction of the guiding molecular dipoles through radiation or other means. © *2011 American Institute of Physics*. [doi:10.1063/1.3663279]

I. INTRODUCTION

There is growing interest in the merging of molecules and electromagnetism.[1–12] The reason is the simultaneous top-down scaling of electromagnetic phenomena from far-field small size nanofeatures, as well as the experimental abilities of bottom-up increase in the size of molecular aggregates. Thus, it is natural that there is a merging region, where molecules can influence electromagnetic features on the nanoscale. This will extend the well-known field of light-matter interaction to near-fields where electromagnetic radiation propagates through nanoplasmons, where molecules can offer new emergent properties of influencing plasmonic fields.

In recent articles,[1–5] we investigated the effect of a single molecule which can direct the motion of electromagnetic radiation between two weakly coupled metal objects (i.e., the molecules can influence plasmon transfer). As this is an example of a small scale polariton (i.e., molecular exciton+plasmon), we labeled it as nanopolaritonics. Here, we extend the treatment to studying effects of a large ensemble of molecules on a single Y-shaped plasmonics structure. We are interested in how selective is the transfer to the molecular density and what is the nature of the resulting spectra. Furthermore, in future articles we will add a layer of control by studying the changes in the transfer as a function of excitation of the molecules by an external laser. This should lead to control of light bending on the nm scale.

Theoretically, the treatment of the combined light+matter problem is a challenging problem due to the differing length scales. However, since the length scales are very small (the size of the studied features is no more than ∼30 nm) we can employ the recent NF (near-field) simulation technique,[13] where only the near-field Poisson-like longitudinal components are considered (this formalism is the time-dependent version of the instantaneous Poisson algorithm in frequency space, e.g., Ref. 14). The main advantage is the time scale which is unrelated to the velocity of light, and therefore is much larger than in the usual Maxwell finite-difference time domain (FDTD) algorithm.[15–17]

Here, we first couple the treatment of metals and of molecules by combining NF with a time-dependent evolution of molecular density matrices (Sec. II). We then study, in Sec. III, the selectivity of plasmonic motion along a Y-shape. The main difference between the physical system here and in the single-molecule studies is the larger transfer as we consider both a single contiguous metal shape as well as a large number of molecules. At low densities there is an overall reduction in transfer, while at higher densities there is an effective hybridization of the molecular and plasmonics field that leads to selectivity, as discussed in the conclusions, Sec. IV.

II. FORMULATION

Below we outline the treatment of the electromagnetic and molecular parts. The overall method is evaluated, in practice, in a leap-frog algorithm where the polarizations and electric fields are evaluated at times 0, dt, 2dt,… while the currents, as well as the molecular density matrices represented later, are represented at times dt/2, 3dt/2, …

A. Electromagnetism: NF

The electromagnetic radiation is treated in the NF (near-field) approximation (for details, see Ref. 13), where the field

is assumed longitudinal; this approximation is valid in the limit where features are much smaller than a wavelength, as employed here, or alternately can be viewed as a $c \to \infty$ approximation. The NF approach is also a time-dependent version of the frequency-based Poisson approach.

The starting point in NF is the assumption that the electric field is the sum of a longitudinal term from a potential with an external field,

$$\mathbf{E}(\mathbf{r}, t) = -\nabla\phi(\mathbf{r}, t) + \mathbf{E}_{ext}(\mathbf{r}, t), \tag{1}$$

where the total potential is obtained from the convolution of an overall charge density, i.e.,

$$\phi(\mathbf{r}, t) = \int \frac{\rho(\mathbf{r}', t)}{|\mathbf{r} - \mathbf{r}'|} d\mathbf{r}'. \tag{2}$$

The overall charge density is obtained from

$$\rho(\mathbf{r}, t) \equiv -\nabla \bullet \mathbf{P}(\mathbf{r}, t). \tag{3}$$

Here, $\mathbf{P}$ is the total polarization. In the article where we introduced NF (Ref. 13), the polarization was purely due to dynamical part of the index of refraction ($\mathbf{P}_p$ below). Here, the polarization also includes the contribution of a molecular layer, $\mathbf{P}_m$,

$$\mathbf{P}(\mathbf{r}, t) = \mathbf{P}_p(\mathbf{r}, t) + \mathbf{P}_m(\mathbf{r}, t). \tag{4}$$

The two contributions to the polarization are discussed below.

The physical limit of NF's validity is that the features considered should be much smaller than (up to ~15%–25% of) a wavelength; in practice,[13] features should be smaller than 50 nm for light in the near-IR to near-UV range. For such small feature sizes retardation effects can be ignored so that the Poisson equation, Eq. (2), could be used. Further, for small feature sizes the transverse contribution to the electric fields due to the vector potential can be ignored.

B. Plasmonic contribution

First, $\mathbf{P}_p(\mathbf{r}, t)$ is evaluated from the electric field by standard FDTD type techniques; i.e., it is formally related to the electric field through a time-dependent kernel,

$$\mathbf{P}_p(\mathbf{r}, t) = \int_{-\infty}^{t} \chi(\mathbf{r}, t - t')\, \mathbf{E}(\mathbf{r}, t') dt', \tag{5}$$

where the more familiar version of this expression is in Fourier space,

$$\mathbf{P}_p(\mathbf{r}, \omega) = (\epsilon(\mathbf{r}, \omega) - \epsilon_0)\mathbf{E}_p(\mathbf{r}, \omega). \tag{6}$$

Then, as usual, the index of refraction for each material is fitted to a Drude form, which makes the calculations convenient, as explained below,

$$\epsilon(\mathbf{r}, \omega) = \epsilon_0 + \epsilon_0 \sum_{j=1}^{N} \frac{\beta_j(\mathbf{r})}{\bar{\omega}_j(\mathbf{r})^2 - \omega^2 - i\omega\alpha_j(\mathbf{r})}. \tag{7}$$

Here, N is a finite number of terms (for gold we use $N = 8$ terms, see Ref. 13 for details). Dielectrics can be handled by an extension, to be discussed in a future article. Equations (6) and (7) are then recast as

$$\mathbf{P}_p = \sum_{j=1,\ldots,N} \mathbf{P}_j, \tag{8}$$

where the individual Lorentzians polarizations fulfill, in frequency space,

$$(\bar{\omega}_j(\mathbf{r})^2 - \omega^2 - i\omega\alpha_j(\mathbf{r}))\mathbf{P}_j(\mathbf{r}, \omega) = \epsilon_0\beta_j\mathbf{E}(\mathbf{r}, \omega), \tag{9}$$

so that their time-evolution equation is

$$\frac{\partial \mathbf{J}_j(\mathbf{r}, t)}{\partial t} = -\alpha_j(\mathbf{r})\mathbf{J}_j(\mathbf{r}, t) - \bar{\omega}_j(\mathbf{r})^2\mathbf{P}_j(\mathbf{r}, t) + \epsilon_0\beta_j\mathbf{E}(\mathbf{r}, t), \tag{10}$$

where

$$\mathbf{J}_j(\mathbf{r}, t) = \frac{\partial \mathbf{P}_j(\mathbf{r}, t)}{\partial t}, \quad j = 1, \ldots, N. \tag{11}$$

Note that $\mathbf{P}_j$, $\mathbf{J}_j$ refer to the plasmonic contribution alone, i.e., they are due to the frequency-dependent part of the index-of-refraction; in principle they should have been denoted as $\mathbf{P}_{p,j}$, $\mathbf{J}_{p,j}$, but we omit the "p" index to avoid cluttering.

The fundamental electrodynamical variables (supplemented by the molecular part below) are therefore the $2N$ vectors, $\mathbf{J}_j(\mathbf{r}, t)$ and $\mathbf{P}_j(\mathbf{r}, t)$, which are propagated by Eqs. (10) and (11). These equations are discretized by a leap-frog algorithm, where the currents and polarizations are given in an alternating time grid, i.e.,

$$\mathbf{J}_j\left(\mathbf{r}, t + \frac{dt}{2}\right) = \frac{1 - \frac{\alpha_j(\mathbf{r})dt}{2}}{1 + \frac{\alpha_j(\mathbf{r})dt}{2}} \mathbf{J}_j\left(\mathbf{r}, t - \frac{dt}{2}\right) - \frac{dt}{1 + \frac{\alpha_j(\mathbf{r})dt}{2}} \left(\bar{\omega}_j^2\mathbf{P}_j(\mathbf{r}, t) - \epsilon_0\beta_j\mathbf{E}(\mathbf{r}, t)\right), \tag{12}$$

and

$$\mathbf{P}_j\left(\mathbf{r}, t + dt\right) = \mathbf{P}_j\left(\mathbf{r}, t\right) + dt\mathbf{J}_j\left(\mathbf{r}, t + \frac{dt}{2}\right). \tag{13}$$

C. Molecular part

The molecular part of the polarization is obtained by evolving the time- and space-dependent density matrices. We denote the local molecular density by $n(\mathbf{r})$ (it could be time-dependent but this is not essential). Then the local molecular polarization is

$$\mathbf{P}_m(\mathbf{r}, t) = n(\mathbf{r})\mathrm{Tr}(\boldsymbol{\mu}(\mathbf{r})D(\mathbf{r}, t)), \tag{14}$$

where we defined the local dipole moment operator and density matrices, respectively. Note the difference between the molecular density $n(\mathbf{r})$ – which is the local number of molecules per volume – and the molecular charge density, defined as

$$\rho_m(\mathbf{r}, t) = -\nabla \cdot \mathbf{P}_m(\mathbf{r}, t). \tag{15}$$

Of course, the two densities are related since the polarization is proportional to the molecular density.

At each point $\mathbf{r}$, the density matrix is propagated using a Liouville equation,

$$i\frac{dD_{ij}(\mathbf{r},t)}{dt} = [F_{\mathbf{E}}(\mathbf{r},t), D]_{ij} - i\Gamma_{ij}\left(\mathrm{D}-\mathrm{D}_0\right)_{ij}, \tag{16}$$

where we introduced the total Fock operator, made from a field-independent part and an electromagnetic component,

$$F_{\mathbf{E},ij}(\mathbf{r},t) \equiv F^0_{ij}(\mathbf{r},t) - \boldsymbol{\mu}_{ij}(\mathbf{r}) \bullet \mathbf{E}(\mathbf{r},t), \tag{17}$$

and $\boldsymbol{\mu}$ is the transition dipole moment (often diagonal in a local basis). Here, we use a field which varies in space but is assumed to be constant over the molecule, corresponding to the dipole approximation; note however that in this formulation the electric field does not need to be locally constant, as the potential within a molecule r_j could have been interpolated from the values on a grid of $\phi(\mathbf{r},t)$, as will be shown in future articles.

For the damping, we take the simplest possible (T_1, T_2) form

$$\Gamma_{ij} = \begin{cases} \frac{1}{T_2} & i \neq j \\ \frac{1}{T_1} & i = j, \end{cases} \tag{18}$$

where now the i,j terms refer to an adiabatic basis.

There are several approaches for propagating the Liouville equation simultaneously with the NF approach – either iterations of Eq. (16) or with exponentials. Two typical approaches used are outlined in the Appendix, and either way propagates $D(\mathbf{r}, t-\frac{dt}{2}) \rightarrow D(\mathbf{r}, t+\frac{dt}{2})$.

Finally, the output of the density matrix propagation is the molecular current,

$$\mathbf{J}_m\left(\mathbf{r}, t+\frac{dt}{2}\right) = -in(\mathbf{r})\mathrm{Tr}([F, D]\boldsymbol{\mu}). \tag{19}$$

The molecular polarization is calculated, for consistency, as

$$\mathbf{P}_m(\mathbf{r}, t+dt) = \mathbf{P}_m(\mathbf{r},t) + dt\mathbf{J}_m\left(\mathbf{r}, t+\frac{dt}{2}\right). \tag{20}$$

D. Propagation summary

The resulting formalism is very simple, and the coupling is through the electric field. It can be summarized as

- After each integer number of time step, $t = ndt$, calculate the total charge density from the combined polarization, Eqs. (3) and (4).
- From the charge density, calculate the potential and then the instantaneous electric field at time $t = ndt$, using Eqs. (1) and (2).
- Then use Eq. (12) to propagate the electrodynamical currents by a single time step to yield, $\mathbf{J}_j(\mathbf{r}, t+\frac{dt}{2})$
- In addition, propagate the molecular current, $\mathbf{J}_m(r, t)$ using the Liouville equation, to get $\mathbf{J}_m(\mathbf{r}, t+\frac{dt}{2})$.
- Use Eqs. (13) and (20) to yield from the resulting electrodynamical and molecular currents to get the polarizations at the next time step, $\mathbf{P}_j(\mathbf{r}, t+dt)$ (where $t+dt = (n+1)dt$), and repeat the cycle.

E. Two-level systems

Here we apply the combined NF-Schrödinger formalism to two-level systems. The zero-field Fock operator is

$$F^0 = \begin{pmatrix} -\frac{\lambda_0}{2} & 0 \\ 0 & \frac{\lambda_0}{2} \end{pmatrix}, \tag{21}$$

and the dipole is off-diagonal in the adiabatic basis,

$$\boldsymbol{\mu} = \begin{pmatrix} 0 & \gamma \\ \gamma & 0 \end{pmatrix}\hat{\mathbf{g}},$$

where $\hat{\mathbf{g}}$ is the direction of the molecule, so the dipole moment is

$$\mathbf{J}_m(\mathbf{r},t) = -2\bar{n}(\mathbf{r})\gamma\lambda_0\hat{\mathbf{g}}\mathrm{Im}D_{12}(\mathbf{r},t). \tag{22}$$

The propagation of the Liouville equation is discussed in the Appendix.

Note that the two-level systems are fully coupled to each other (i.e., there is full exciton-exciton coupling) because they interact with the total electric field, and therefore with the total potential, which in turn has a component due to the underlying molecular density variation in space. To see this explicitly, note that the full potential, Eq. (1), can be divided to plasmonic and molecular contributions

$$\begin{aligned}\phi(\mathbf{r},t) = \phi_p + \phi_m &= \int \frac{\rho_p(\mathbf{r}',t)}{|\mathbf{r}-\mathbf{r}'|}d\mathbf{r}' + \int \frac{\rho_m(\mathbf{r}',t)}{|\mathbf{r}-\mathbf{r}'|}d\mathbf{r}' \\ &= -\int \frac{\nabla \bullet \mathbf{P}_p(\mathbf{r}',t)}{|\mathbf{r}-\mathbf{r}'|}d\mathbf{r}' - \int \frac{\nabla \bullet \mathbf{P}_m(\mathbf{r}',t)}{|\mathbf{r}-\mathbf{r}'|}d\mathbf{r}',\end{aligned} \tag{23}$$

where the respective potentials and densities are defined by the equation. Equation (23) shows clearly that the molecules are coupled to each other's polarization, so that even if there is no metal the formalism could still be used to describe the local exciton-exciton coupling.

F. Initial conditions

The initial conditions are straightforward; the currents and polarizations vanish, and the density matrix is at its equilibrium value

$$\mathbf{P}_j(\mathbf{r}, t=0) = \mathbf{P}_m(\mathbf{r}, t=0) = 0,\ \mathbf{J}_j\left(t = -\frac{dt}{2}\right) = 0,$$

$$D(\mathbf{r}, t=0) = \begin{pmatrix} 1 & 0 \\ 0 & 0 \end{pmatrix}.$$

The only nonvanishing part is the external field. It is simplest to use a delta function in time,

$$\mathbf{E}_{ext}(\mathbf{r},t) = \mathbf{E}_{0,ext}(\mathbf{r})\delta(t), \tag{24}$$

i.e.,

$$\mathbf{E}_{ext}(\mathbf{r}, n\,dt) = \begin{cases} \frac{\mathbf{E}_{0,ext}(\mathbf{r})}{dt} & n = 0 \\ 0 & n > 0. \end{cases}$$

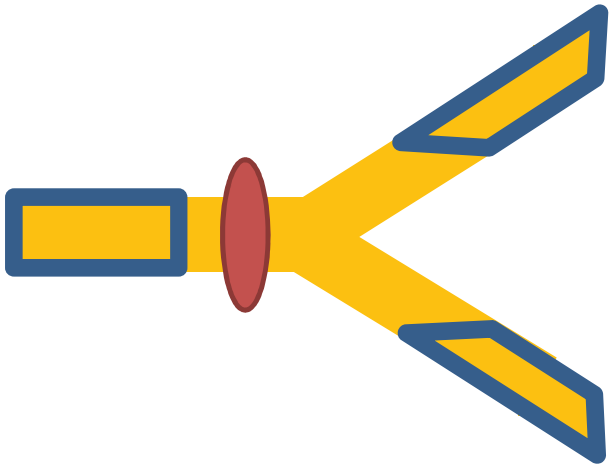

FIG. 1. Schematic drawing of the metal gold Y-shape. An external electric field pulse is applied on the left (red circle), and the surrounding molecular medium influences the direction the current takes (up or down). The boxed regions indicate where the currents are measured (back, up, and down, respectively).

Since we are interested in propagation, we apply a Gaussian pulse in the x-direction,

$$\mathbf{E}_{0,ext}(x,y,z) = E_0 \exp\left(-\frac{(x-x_0)^2}{\Delta^2}\right)\hat{\mathbf{x}}.$$

As long as the initial field is sufficiently small, the results are independent of it (i.e., in the linear response regime), so we used $E_0 = 0.0001$ a.u.

III. APPLICATIONS

We apply the formalism to a Y-shape system (see Fig. 1 for schematics). Within the Y-shape, we use the Drude parameters for gold from Ref. 13 Other parameters are delineated in Table I and below.

The initial electric field pulse is applied along the x-direction, and the resulting summed current is measured along the two outlying directions (up and down), i.e., the upper and lower quarters of the grid, as well as the back part (see Fig. 1),

$$E_u \equiv \int |\mathbf{J}(\mathbf{r},\omega)|^2 \theta\left(y - \frac{y_{\max}}{2}\right) d\mathbf{r},$$

$$E_d \equiv \int |\mathbf{J}(\mathbf{r},\omega)|^2 \theta\left(\frac{y_{\min}}{2} - y\right) d\mathbf{r},$$

$$E_{back} \equiv \int |\mathbf{J}(\mathbf{r},\omega)|^2 \theta\left(\frac{x_{\min}}{2} - x\right) d\mathbf{r},$$

where we presumed the origin is at the center of the grid. The results were scaled overall, as they depend linearly on the initial current. The integrated intensity of the current is not exactly the total energy, which depends on the dielectric constant, but is indicative of the transmission.

Most calculations were done with a grid spacing of 0.5 nm; we checked that a $(64 \times 64 \times 32)$ grid was sufficient. The Y-shape parameters are delineated in the table.

Further, in most calculations the molecules were presumed to be oriented along the $\hat{\mathbf{g}} = (1,1,0)/\sqrt{2}$ direction. The maximum molecular absorption is for an energy of $\lambda_0 = 1.36$ eV, and the molecule has a mildly narrow absorption feature, with $T_2 = 14.5$ fs, associated with a width of $1/T_2 = 0.045$ eV. We used $T_1 = 4\ T_2$, but it generally made little difference since it is quite large.

Two cases are considered: molecules which fill all space outside the fork shape (so $\bar{n}(\mathbf{r})$ is constant in space outside the fork) and a separate case where the molecules coat the fork. In the coated-fork case the molecules extend beyond the perpendicular directions (y,z) of the fork by 1.25 nm; i.e., for each point in space which is outside the fork but within a distance of 1.25 nm in y and z from the fork surface, $\bar{n}(\mathbf{r})$ is constant; outside that coating (and also within the metal fork itself) $\bar{n}(\mathbf{r})$ vanishes.

The crucial parameters are the molecular density and transition dipole moments. Figure 2 shows the resulting transmission as a function of frequency for several molecular densities and a transition dipole moment fixed at 2 a.u. In this figure, the molecular density is coated on the Y-shape; the coating width, 1.25 nm, is below the width of the Y-shape (5 nm in the out-of-plane axis z, and 3.1 nm, and 2 nm for the incoming and outgoing arms, respectively, in the y-direction). However, the results scale with geometry due to the Poisson NF method used, so that identical-looking figures will emerge if the Y-shape size and coating would have been multiplied by any constant factor, as long as the overall features are much smaller than a wavelength.

As a comparison, Figure 3 shows the transmission for a related case where now the molecules fill the whole space (i.e., the whole grid). The two figures show several interesting trends.

First, higher density is required in the coated case, as expected as it involves fewer molecules, although in both cases the densities are low (0.7–13 vs. 3–27 molecules per nm^3 for the space-filling and coated cases, respectively).

Second, the behavior with density is reminiscent of an hybridization[18] between the molecular degree of freedom and the plasmon resonance,[1,10] and the hybridization is proportional to the molecular density which is the linear parameter coupling the two regions.

TABLE I. Parameters. All distances are in nm, but the results scale if all distances are scaled up or down as long as the overall dimension is significantly smaller than a wavelength. Other parameters are described in the results section.

Y-shape left arm: length × width × depth	16 × 3.1 × 5
Right arm: length × width × depth	10 ×2 × 5
Angle between Y-shape arms	101^0
Time step	2.5 a.u.∼ 0.07 fs
Grid spacing, dx	0.5
Pulse width, Δ	2
x_{max},y_{max},z_{max}	dx/2 * (64-1,64-1,32-1)
Dt	3 a.u.
dt_m	0.5 a.u.

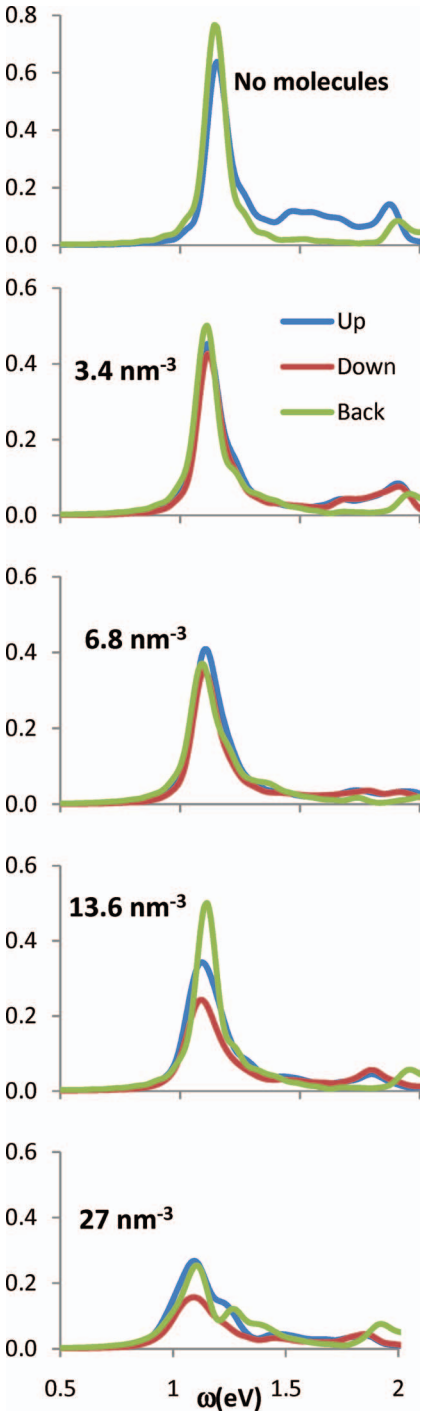

FIG. 2. Coated Y-shape; energies (scaled overall) in the two Y-shape arms (up and down) and in the back arm as a function of frequency for a Y-shape coated with molecules, for several molecular densities.

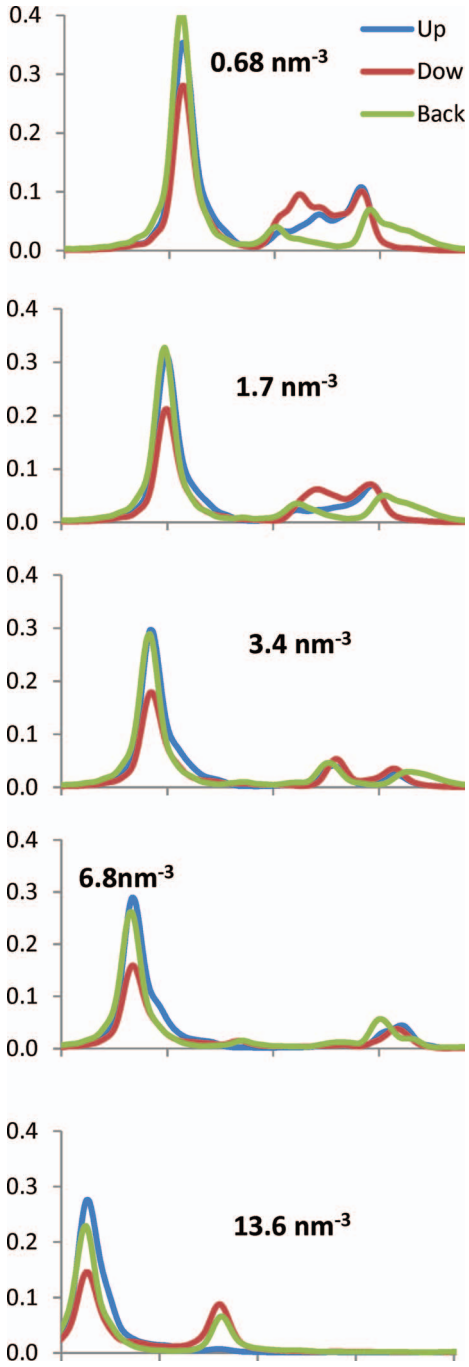

FIG. 3. Space-filling molecules: Analogous to Fig. 2, but for a space-filled with molecules. Here, a discernible gating effect (up vs. down) is evident at lower densities, and there is stronger redshifting. Note the smaller peak at the highest density, expanded in Fig. 4.

Third, for the coated case, at low molecular densities the dominant effect is not the selectivity, but is instead a reduction of the overall absorption. This is understandable since most of the molecules are not in the transition region near the Y-shape center, so that they affect the transmission similarly but just cause a change in the effective dielectric constant, leading to a change in the absorption feature.

Figure 4 shows an expanded part of Fig. 3 at frequencies between 1–1.5 eV, for a high molecular density (27 molecules per nm^3). Interestingly, in this case very high selectivity results in this particular frequency range. We speculate that this is due to the overlap of this region with the molecular resonance. Specifically, note that in this case the plasmonics current is damped in the direction of the molecular dipole (positive-x-positive-y), pointing to a possible interference effect at these frequencies.

Finally, we compare in Fig. 5 the overall molecular-current squared to the squared plasmonics current,

$$\int |\mathbf{J}_m(\mathbf{r},\omega)|^2 d\mathbf{r}, \quad \int |\mathbf{J}_p(\mathbf{r},\omega)|^2 d\mathbf{r}$$

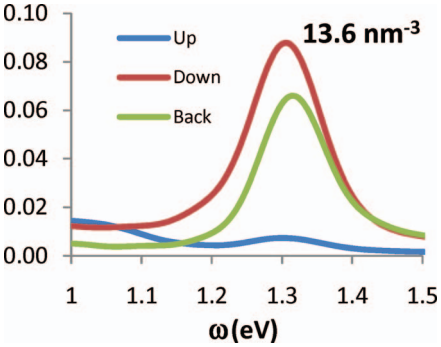

FIG. 4. An expanded view of Fig. 3 for a high molecular density case. Very strong selectivity emerges due to the interaction with the molecular resonance at 1.36 eV.

(where the molecular parts includes the density, squared in the formula), for the coated case, at two densities. As noted, the molecular current can be quite appreciable, but is generally at higher frequencies.

IV. DISCUSSION

The simulations presented here show several properties. First, molecular coating and dielectric effects can markedly influence the selectivity of transport of plasmons in the nanoregime, This effect has been advocated for smaller molecules (even single molecule) for the weaker transport between two metal structures; here, a continuous structure is taken, so a larger number of molecules is used.

Second, the most important lesson is how little molecular density is needed to affect the direction to which light is scattered. The overall densities needed are quite small; in fact, at higher densities the molecular currents will dominate over the plasmonics currents, due to the larger number of electrons per molecule.

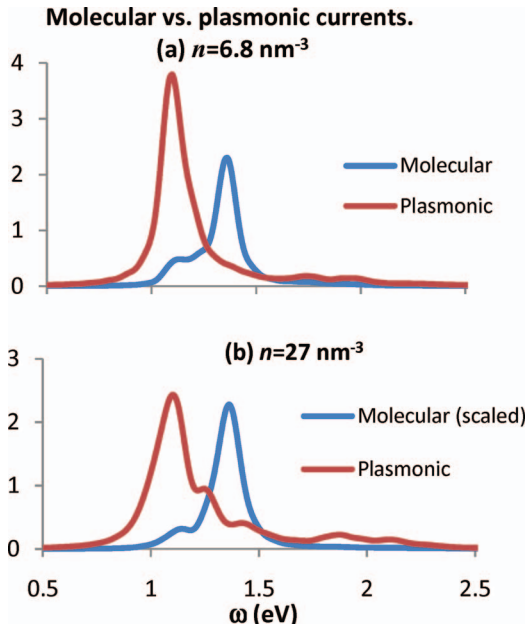

FIG. 5. Molecular vs. plasmonics currents for the coated case, for two densities; for the higher molecular density, the molecular current is scaled down (by a factor of 16) for easier comparison to the plasmonics current.

In the small-feature limit, which is way below a wavelength, the results scale completely with the size of the features (i.e., the overall currents are unchanged when the densities are fixed and the geometries are scaled up or down). Thus, our results have general validity through a large range of nanofeatures, from ∼2 nm (above which the Maxwell local susceptibility approximation is expected to make sense) all the way to overall feature sizes as larger as ∼50 nm.

Third, an interesting feature is the shift of the plasmon resonances with increasing density, especially when the molecules fill the space (rather than coated) – the overall shift starts at lower densities, while at higher densities selectivity emerges. This is because the overall shift is controlled by the dielectric constant effects on the full plasmon, while the selectivity is controlled by the response near the center of the Y-shape where the electric fields split.

Finally, we note that while the simulations with gold resulted in IR frequency absorption, different materials will shift the overall frequencies from the IR to optical and even UV region. Such shifts could be used to switch light into different cutoff waveguides or spectral filters. Light control shifts will allow, as mentioned above, to switch "light by light" (or through other means such as change of pH, or electrically) on the nanoscale.

ACKNOWLEDGMENTS

D.N. is grateful for very fruitful discussions with Shimon Weiss and for support by the National Science Foundation (NSF).

APPENDIX: 2-LEVEL PROPAGATION

The two-level systems is propagated here, $D(t-\frac{dt}{2}) \to D(t+\frac{dt}{2})$, by splitting the molecular time step, dt, to M finer steps

$$dt_m = \frac{dt}{M},$$

and then applying one of the two approaches. The simplest is to apply M times,

$$D \to D + dt_m \frac{dD}{dt}.$$

Alternately, for a two-level system, we can use a three-step part; in the first step the effect of the damping over half-time step is calculated as

$$\tilde{D}\left(t-\frac{dt_m}{2}\right) = W\left(D\left(t-\frac{dt_m}{2}\right)\right),$$

where the matrix operator W is defined as

$$\tilde{D}_{ij}\left(t-\frac{dt_m}{2}\right) = \begin{cases} \exp\left(-\frac{dt_m}{2T_2}\right) D_{ij}\left(t-\frac{dt_m}{2}\right) & i \neq j \\ \exp\left(-\frac{dt_m}{2T_1}\right) D_{22}\left(t-\frac{dt_m}{2}\right) & i=j=2\cdot \\ 1-\tilde{D}_{22}\left(t-\frac{dt_m}{2}\right) & i=j=1 \end{cases} \tag{A1}$$

Then the Fock part is propagated as

$$D'\left(t+\frac{dt_m}{2}\right)=U\tilde{D}\left(t-\frac{dt_m}{2}\right)U^{\dagger}$$

where

$$U=\exp\left(-i\frac{dt_m}{2}F\right). \tag{A2}$$

For 2-level systems, we use a Pauli matrix notation for the Fock operator,

$$\begin{aligned} &Fdt_m=-\boldsymbol{\mu}\bullet\mathbf{E}(\mathbf{r},t)dt_m\sigma_x-\frac{\lambda dt_m}{2}\sigma_z=\mathbf{v}\bullet\sigma,\\ &\mathbf{v}=\left(-\boldsymbol{\mu}\bullet\mathbf{E},0,-\frac{\lambda}{2}\right)dt_m=v\hat{\mathbf{v}},\\ &v\equiv dt_m\sqrt{(\boldsymbol{\mu}\bullet\mathbf{E})^2+\frac{\lambda^2}{4}}, \end{aligned} \tag{A3}$$

so that

$$\begin{aligned} U&=\exp\left(-i\mathbf{v}\bullet\sigma\right)=\cos\left(v\right)\mathbf{I}-i\sin\left(v\right)\hat{\mathbf{v}}\bullet\sigma\\ &=\cos\left(v\right)\mathbf{I}-i\frac{\sin\left(v\right)}{v}Fdt_m, \end{aligned}$$

and finally the density matrix is damped again using the same transformation as before,

$$D\left(t+\frac{dt_m}{2}\right)=W\left(D'\left(t+\frac{dt_m}{2}\right)\right).$$

[1] D. Neuhauser and K. Lopata, J. Chem. Phys. **127**(15), 154715 (2007).
[2] K. Lopata and D. Neuhauser, J. Chem. Phys. **131**(1), 014701 (2009).
[3] K. Lopata and D. Neuhauser, J. Chem. Phys. **130**(10), 104707 (2009).
[4] C. Arnsten, K. Lopata, M. R. Wall, L. Bartell, and D. Neuhauser, J. Chem. Phys. **134**(08), 084101 (2011).
[5] D. Neuhauser, C. Arnsten, and K. A. Lopata, *Encyclopedia of Nanotechnology*, edited by B. Bhushan (Springer, New York, 2012) (to be published).
[6] Y. B. Zheng, Y.-W. Yang, L. Jensen, L. Fang, B. K. Juluri, A. H. Flood, P. S. Weiss, J. F. Stoddart, and T. J. Huang, Nano Lett. **9**(2), 819 (2009).
[7] A. A. Lazarides, K. Lance Kelly, T. R. Jensen, and G. C. Schatz, J. Mol. Struct.: THEOCHEM **529**(1–3), 59 (2000).
[8] J. Y. Yan, W. Zhang, S. Q. Duan, X. G. Zhao, and A. O. Govorov, Phys. Rev. B **77**(16), 165301 (2008).
[9] J. Lee, P. Hernandez, J. Lee, A. O. Govorov, and N. A. Kotov, Nature Mater. **6**(4), 291 (2007).
[10] N. T. Fofang, T.-H. Park, O. Neumann, N. A. Mirin, P. Nordlander, and N. J. Halas, Nano Lett. **8**(10), 3481 (2008).
[11] D. J. Masiello and G. C. Schatz, J. Chem. Phys. **132**(6), 064102 (2010).
[12] M. Sukharev and M. Galperin, Phys. Rev. B **81**, 165307 (2010).
[13] A. Coomar, C. Arntsen, K. A. Lopata, S. Pistinner, and D. Neuhauser, J. Chem. Phys. **135**(8), 084121 (2011).
[14] Y. Sivan, S. Xiao, U. K. Chettiar, A. V. Kildishev, and V. M. Shalaev, Opt. Express **17**(26), 24060 (2009).
[15] A. Taflove and S. Hagness, *Computational Electrodynamics : The Finite-Difference Time-Domain Method*, 2nd ed. (Artech House, Boston, MA, 2000).
[16] C. Girard, Rep. Prog. Phys. **68**(8), 1883 (2005).
[17] S. K. Gray and T. Kupka, Phys. Rev. B **68**(4), 045415 (2003).
[18] E. Prodan, C. Radloff, N. J. Halas, and P. Nordlander, Science **302**(5644), 419 (2003).